Materials Today Energy 36 (2023) 101356

Contents lists available at ScienceDirect

Materials Today Energy

journal homepage: www.journals.elsevier.com/materials-today-energy/

Development of P3-type $K_{0.70}[Cr_{0.86}Sb_{0.14}]O_2$ cathode for high-performance K-ion batteries

Wonseok Ko [a, b, e], Junseong Kim [a, b, e], Jungmin Kang [a, b], Hyunyoung Park [a, b], Yongseok Lee [a, b], Jinho Ahn [a, b], Bonyoung Ku [a, b], Myungeun Choi [a, b], Hobin Ahn [a, b], Gwangeon Oh [d], Jang-Yeon Hwang [d, e, **], Jongsoon Kim [a, b, c, *]

[a] Department of Energy Science, Sungkyunkwan University, Suwon 440-746, Republic of Korea
[b] SKKU Institute of Energy Science and Technology (SIEST), Sungkyunkwan University, Suwon 440-746, Republic of Korea
[c] KIST-SKKU Carbon-Neutral Research Center, Sungkyunkwan University, Suwon 16419, Republic of Korea
[d] Department of Energy Engineering, Hanyang University, Seoul 04763, Republic of Korea
[e] Department of Battery Engineering, Hanyang University, Seoul 04763, Republic of Korea

ARTICLE INFO

Article history:
Received 10 April 2023
Received in revised form
9 June 2023
Accepted 21 June 2023
Available online 26 June 2023

Keywords:
Cathode material
Layered-type structure
Potassium-ion battery
First-principles calculation

ABSTRACT

Potassium-ion batteries (KIBs) are one of the most promising alternatives to lithium-ion batteries because of the high standard hydrogen electrode of K^+/K, which is the second lowest after lithium. However, the large ionic size of K^+ generally hinders the reversible intercalation and results in the undesirable structural changes during charge-discharge process. Thus, it is very important to develop stable cathode materials that accommodate K^+ into their crystal structure with minimal structural changes. Here we propose P3-type $K_{0.70}$ $[Cr_{0.86}Sb_{0.14}]O_2$ as a potential cathode material for high-performance KIBs. The P3-type $K_{0.70}$ $[Cr_{0.86}Sb_{0.14}]O_2$ was successfully fabricated via electrochemical ion-exchange of Na^+/K^+. At a current density of 15 mA/g, P3−$K_{0.70}$ $[Cr_{0.86}Sb_{0.14}]O_2$ delivered a reversible capacity of 126.1 mAh/g with a high coulombic efficiency of 98.7%, corresponding to the de/intercalation of 0.57 mol of K^+ ions from/into the structure. In addition, P3-type $K_{0.70}$ $[Cr_{0.86}Sb_{0.14}]O_2$ showed excellent cycling stability over 200 cycles at a current density of 150 mA/g and power capability even at high current rate of 750 mA/g. In contrast, P3-K_xCrO_2 demonstrates inferior electrochemical properties; this comparison implies that substitution of 0.14 mol Sb into Cr sites significantly improves structural stability with reversible $Cr^{3+/4+}$ redox reaction during charge-discharge process.

1. Introduction

As the energy storage systems for various electronic devices and electric vehicles (EVs), lithium-ion batteries (LIBs) have been achieved great attention, and their demands are explosively increasing [1–3]. However, due to the limited reliability of lithium resources, there may be difficulties in smoothly producing lithium-ion batteries to meet worldwide demands, which could ultimately result in high costs for LIBs in the near future [4–6]. Thus, for grid-scale applications such as EVs, it is important to develop non-lithium-based cost-effective rechargeable batteries [7,8].

Recently, potassium-ion batteries (KIBs) are one of the most promising alternatives to LIBs, owing to the earth-abundant potassium resources. KIBs can offer a relatively high energy density compared to other cost-effective rechargeable batteries such as sodium-ion batteries and zinc-ion batteries, due to the lower redox potential of K^+/K (−2.93 V vs. standard hydrogen electrode (*SHE*)) compared to Na^+/Na (−2.71 V *vs. SHE*) and Zn^{2+}/Zn (−0.76 *vs. SHE*) [8–12]. Moreover, it is known that potassium ions (K^+) can be intercalated into the graphite structure [13]. This implies that graphite, which is conventionally used as the anode material for lithium-ion batteries (LIBs), can also be utilized as an anode material for potassium-ion batteries (KIBs). This connection allows for the seamless integration of KIBs into the existing LIB industry [11,13–16]. Therefore, many researches have focused on various

* Corresponding author.
** Corresponding author.
E-mail addresses: jangyeonhw@hanyang.ac.kr (J.-Y. Hwang), jongsoonkim@skku.edu (J. Kim).
[e] These authors contributed equally to this work.

https://doi.org/10.1016/j.mtener.2023.101356
2468-6069/

researches of cathodes and electrolytes for KIBs [16–18]. Especially, various types of cathode materials have been reported, such as transition metal oxides, polyanion compounds, Prussian blue analogues, and etc [19–22].

Among them, it has been reported the layered-type potassium transition metal oxides 'K_x [TM]O_2' (where TM stands for a transition metal) can have a large gravimetric capacity and energy density due to their low molar mass [23,24]. However, the large ionic size of K^+ (~1.38 Å) compared to that of Li^+ (~0.76 Å) leads to the significant structural changes during K^+ de/intercalation within the structure [4,25,26]. Thus, K_x [TM]O_2 exhibited a smaller reversible capacity during charge/discharge compared to its theoretical capacity, and its voltage profile was composed of multiple steps. These characteristics are considered to be the major drawbacks of K_x [TM]O_2 cathode materials. In terms of P3-type K_xCrO_2 (P3–KCO), its theoretical capacity is close to ~200 mAh/g, but as reported, its actual discharge capacity was only ~100 mAh/g in the voltage range of 1.5–3.8 V (vs. K^+/K) accompanied by a multiple-step-based charge/discharge curve [26]. To enhance the discharge capacity and energy density, it is essential to improve the stability of the layered structure to prevent the large and severe structural changes during charge/discharge. It has been reported that the substitution of metal ions with fixed valence states in the structure can play a role as a structural stabilizer, resulting in successful improvements in the structural stability and electrochemical performances of layered-type oxide cathode materials [27–29].

Herein, we demonstrated that the substitution of 0.14 mol of Sb^{5+} with a fixed valence state during charge/discharge can successfully enhance the electrochemical properties of P3–KCO under the KIB system. Sb-substitution has been used for enhancing the electrochemical performances of cathode materials. Particularly, substitution of Sb^{5+} with high electronegativity enables the strong bonding with neighboring oxygen atoms. Moreover, Sb^{5+} in the cathode does not participate in the electrochemical reactions during charge/discharge. Thus, we expected that Sb^{5+} can acts as a stabilizer by mitigating the structural changes associated with K^+ de/intercalation at the structure [30,31]. Through combined studies using first-principles calculations and electrochemical tests, it was confirmed that ~0.53 mol of K^+ corresponding to the capacity of ~126 mAh/g can be reversibly de/intercalated in the P3–$K_{0.70}$[$Cr_{0.86}Sb_{0.14}$]O_2 (P3–KCSO) structure in the voltage range of 1.5–4.1 V (vs. K^+/K). In particular, the charge/discharge curve of P3–KCSO was composed of simple, smooth curve without multiple steps, which is clearly distinct from that of P3–KCO. Moreover, as a promising cathode material for KIBs, P3–KCSO exhibited outstanding power-capability and cycle-performances. Even at a current density of 750 mA/g, the discharge capacity of P3–KCSO was ~88.9 mAh/g corresponding to a capacity retention of ~71.1% compared to the capacity measured at 15 mA/g, whereas P3–KCO only delivered ~45.6 mAh/g under the same conditions. For 200 cycles at 150 mA/g, the specific capacity of P3–KCSO was retained up to ~92.4% compared to the initial capacity. In addition, the structural stability and reaction mechanism of P3–KCSO under the KIB system were confirmed through *operando* X-ray diffraction (XRD) and *ex situ* synchrotron-based X-ray absorption spectroscopy (XAS) analyses.

2. Experimental

2.1. Preparation of $NaCrO_2$ and $Na_{0.72}Cr_{0.86}Sb_{0.14}O_2$

Before the ion-exchange process for P3–KCO and P3–KCSO, $NaCrO_2$ and $Na_{0.72}Cr_{0.86}Sb_{0.14}O_2$ were synthesized via the solid-state method. Na_2CO_3 (purity: 99.5%), Cr_2O_3 (purity: 98.5%) and $CrSbO_4$ were used as precursors and mixed with desired ratio using a planetary ball-mill for 500 rpm for 12 h, with 10 wt % excess of Na_2CO_3 to compensate for losses during calcination process. After mixing, we made pellets using the mixed powders and calcined them at 900 °C for 10 h using an Ar gas flowed (0.8 L/min) tube furnace.

After synthesis, O3–$NaCrO_2$ and $Na_{0.72}Cr_{0.86}Sb_{0.14}O_2$ were carbonized using pyromellitic acid ($C_{10}H_6O_2$: PA, purity: 96%) to improve the electrical conductivity and provide the buffer to prevent the large structural change during charge/discharge. Mixed each bare powders and PA pressed to make each pellet, and these pellets were transferred to Ar gas flowed tube furnace and heated for 30 min at 550 °C. The weight ratio of cathode: carbon in the carbon-coated cathodes is 85: 15.

In this synthesis system, we used $CrSbO_4$ as a precursor instead of antimony oxide. If antimony oxide is used instead of $CrSbO_4$, antimony is not doped and reacts separately with sodium, because the reactivity of chromium oxide is low. To prepare $CrSbO_4$, a mixture of Cr_2O_3 and Sb_2O_4 (Sb(III) + Sb(V)) was used, with Sb_2O_4 obtained by heat treating Sb_2O_3 (purity: 99.5%) at 550 °C for 10 h in air. The Cr_2O_3 and Sb_2O_4 were mixed in a 1:1 M ratio using high-energy ball-milling at 400 rpm for 12 h, followed by heating at 600 °C for 3 h and 1050 °C for 10 h in air.

2.2. Na^+/K^+ ion-exchange process

We prepared P3–KCO and P3–KCSO through a Na^+/K^+ ion-exchange process using electrochemical reactions under the K-system since they are difficult to synthesize directly via a solid-state method. Electrodes of O3–$NaCrO_2$ and $Na_{0.72}Cr_{0.86}Sb_{0.14}O_2$ were prepared and assembled into K-cell, and charged/discharged within a voltage range of 1.5–3.8 V ($NaCrO_2$) or 1.5–4.1 V ($Na_{0.72}Cr_{0.86}Sb_{0.14}O_2$) for 100 cycles at 300 mA/g. After cycling, the coin cells were disassembled in an Ar-filled glove box, and the resulting electrodes were washed with dimethyl carbonate (DMC) five times and then dried.

2.3. Materials characterization

The crystal structure and information were analyzed using X-ray diffraction (XRD) with Mo Kα radiation (λ = 0.70930 Å) on a PANalytical Empyrean instrument. Structural data were collected over the 2θ range of 4.6°–34.3° with a step size of less than 0.01°. For XRD analysis powder samples were directly used, but electrode samples were sealed with Kapton tape to prevent air and moisture contact. The collected XRD patterns were converted to fit the Cu Kα radiation (λ = 1.54178 Å). Rietveld refinement was performed using FullProf software. High-resolution transmission electron microscopy (HR-TEM; JEM-F200 at the National Center for Interuniversity Research Facilities (NCIRF) at Seoul National University) was performed at accelerating voltages of 80–120 kV. The Cr K-edge X-ray absorption spectroscopy (XAS) spectra was obtained at beamline 7D at the PAL using Cr metal foils as references.

2.4. Electrochemical characterization

To preparation of electrode, carbon-coated cathode, Super-P and polyvinylidene fluoride (PVDF) were mixed in an 82.35 : 7.65: 10 wt ratio with N-methyl-2-pyrrolidone (NMP), and the mixed slurry was applied onto Al foil with 200 μm thickness, and dried in a vacuum oven at 100 °C. After dried, the mass loading of the active material on the Al foil was ~3×10^{-3} g/cm^2. The total weight ratio of cathode (in coated powder): coated carbon (in coated powder) + Super-P: PVDF in the electrode is as follows; 70 (82.35 × 0.85): 20 (82.35 × 0.15 + 7.65): 10.

All electrochemical reaction were performed using an automatic battery charge/discharge test system (WBCS 3000, WonATech) under same K-system. R2032-type coin cell parts were used, and all coin cells were assembled in Ar-filled glove box. To assemble the coin cell, electrodes were punched into 10π-mm diameter disks, and Whatman GF/F glass fiber filter, 0.5 M of KPF_6 in a 1:1 v/v mixture of ethylene carbonate (EC), and diethyl carbonate (DEC), and K-metal were used as the separator, electrolyte and counter electrode respectively.

2.5. Computational details

The density functional theory calculations in this work were performed using the Vienna Ab initio Simulation Package (VASP) and projector-augmented wave (PAW) method. For the exchange correlation functional, we utilized the Perdew–Burke–Ernzerhof (PBE) parametrization of the generalized gradient approximation (GGA). The supercell structure of $K_xCr_{0.86}Sb_{0.14}O_2$ was set as $2 \times 2 \times 1$, and a k-point grid of $5 \times 5 \times 2$ was used. The GGA + U method was adopted to address the localization of the d-orbital in Cr ions, with a U eff value of 3.7 eV as used in previous studies [5,28,32]. A kinetic energy cutoff of 500 eV was used in all the calculations, and all the structures were optimized until the force in the unit cell converged to within 0.03 eV $Å^{-1}$. CASM software was used to generate all the K^+/vacancy configurations for each composition, followed by full DFT calculations on a maximum of 20 configurations with the lowest electrostatic energy for each composition used to obtain the convex-hull plot of $K_xCr_{0.86}Sb_{0.14}O_2$.

3. Results and discussion

P3–K0.70 [Cr0.86Sb0.14]O2 (P3–KCSO) and P3-type KxCrO2 (P3–KCO) were prepared through an Na^+/K^+ ion-exchange process using electrochemical reactions under the K-system, since they are difficult to synthesize directly via a solid-state method. Electrodes of O3-type $NaCrO_2$ (O3–NCO) and $Na_{0.72}$ $[Cr_{0.86}Sb_{0.14}]O_2$ (O3–NCSO) were prepared and assembled into K-cells, and charged/discharged within a voltage range of 1.5–3.8 V (O3–$NaCrO_2$) or 1.5–4.1 V (O3–$Na_{0.72}$ $[Cr_{0.86}Sb_{0.14}]O_2$) for 100 cycles at 300 mA/g. After cycling, the coin cells were disassembled in an Ar-filled glove box, and the resultant electrodes were washed with dimethyl carbonate (DMC) five times and then dried. To investigate the structural information of P3–KCSO, we performed Rietveld refinement based on the XRD pattern. As shown in Fig. 1a, it was verified that P3–KCSO is composed of the pure P3-type layered structure with *R3m* space group, which is clearly different from the crystal structure of O3–NCSO (Fig. S1 Table S1). The lattice parameters of *a* and *c* of P3–KCSO were ~2.9423 (2) Å and 18.606 (3) Å, respectively. The low values of the reliable factors ($R_P = 3.44\%$, $R_I = 5.07\%$, $R_F = 5.44\%$, $\lambda^2 = 2.73\%$) indicate the high accuracy of the Rietveld refinement on P3–KCSO. The detail structural information, such as atomic positions, isotropic parameters, and occupancies of K, Cr, Sb and O, are tabulated in Table S2. Moreover, as the results of Rietveld refinement, it was verified that ~0.70 mol of K^+ exists in the structure of P3–KCSO, which was consistent with the inductively coupled plasma (ICP) results (Table S3). These results imply that the atomic ratio of K: Cr: Sb in P3–KCSO was ~0.70 : 0.86: ~0.14, and no Na elements were detected. Since Sb cation has higher valence states of +5 than Cr cation with the valence states of +3, the K^+ contents in P3-K_x $[Cr_{0.86}Sb_{0.14}]O_2$ should be no more than 0.72 mol for the charge neutrality. Thus, 0.7 mol K^+ contents can exist in P3–$K_{0.7}$ $[Cr_{0.86}Sb_{0.14}]O_2$ after 0.14 mol Sb-substitution. To prepare the P3–KCSO without residual Na contents in the structure

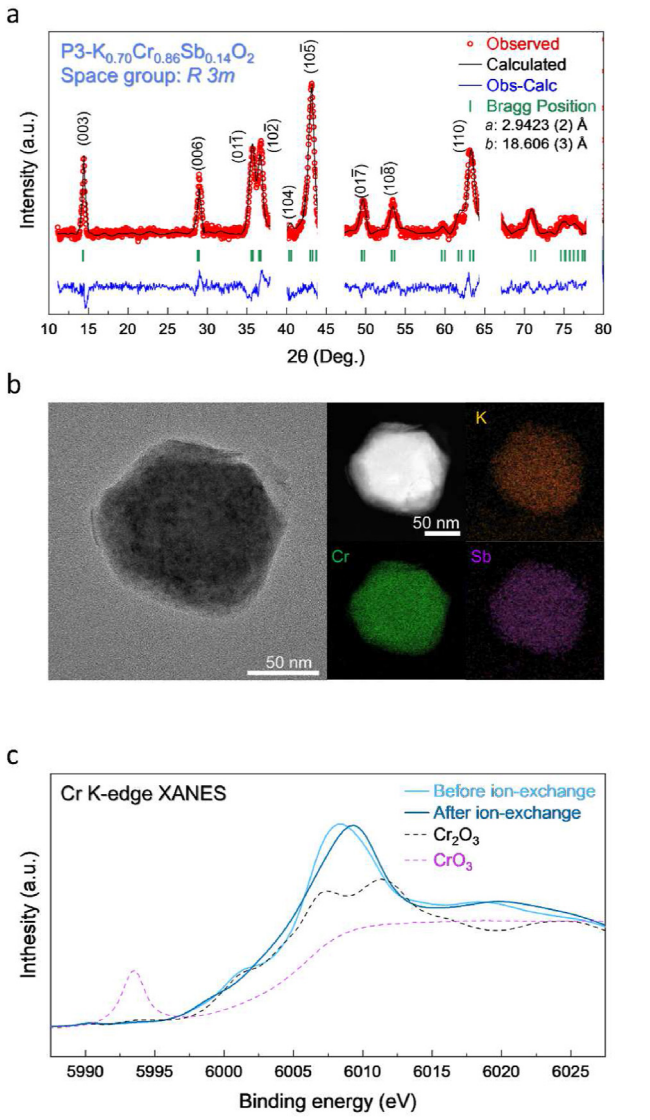

Fig. 1. (a) Rietveld refinement of the XRD pattern of P3–$K_{0.70}Cr_{0.86}Sb_{0.14}O_2$. (b) TEM image and TEM–EDS mapping of the P3–$K_{0.70}Cr_{0.86}Sb_{0.14}O_2$. (c) Cr K-edge of O3–$Na_{0.72}Cr_{0.86}Sb_{0.14}O_2$ and P3–$K_{0.70}Cr_{0.86}Sb_{0.14}O_2$ electrodes.

through the electrochemical ion-exchange process, many times of charge/discharge cycling should be required. As shown in Fig. S2, it was verified that the O3-type phase was gradually disappeared during cycles and the P3-type phase was simultaneously formed, which implies the occurrence of ion-exchange process from O3–NCSO to P3–KCSO. After 100 cycles, the O3-type phase was perfectly transformed into the P3-type phase, indicating that 100 cycles under the KIB system should be required to prepare the P3–KCSO. In addition, we compared the elemental ratio of pristine and 50-cycled sample using the ICP analyses. As shown in Table S4, the residual Na contents still exist in the 50-cycled sample and there are negligible Na contents in the 100-cycled sample (=P3–KCSO, Table S3). We also investigated the morphology and atomic ratio of P3–KCSO using High-resolution transmission electron microscopy (HR-TEM) and energy-dispersive X-ray spectroscopy (EDS) analyses. As shown in Fig. 1b, the particle size of P3–KCSO was ~130 nm, and K, Cr, and Sb elements were homogenously distributed in the particles with the an atomic ratio of

~0.70: ~0.86: ~0.14. In addition, Fig. 1c shows the X-ray absorption near edge structure (XANES) analyses, which indicate that the oxidation state of Cr in P3−KCSO was +3, implying K^+ in P3−KCSO can be de/intercalated through redox reaction of Cr^{3+}/Cr^{4+}.

To understand the theoretical electrochemical reaction occurred in P3−KCSO under the KIB system, we performed first-principles calculation. We prepared various K^+/vacancies configurations of P3-K_x $[Cr_{0.86}Sb_{0.14}]O_2$ compositions (K = 0, 0.25, 0.5, 0.75, 1) using cluster-assisted statistical mechanics (CASM) software. Subsequently, we plotted the convex hull based on their relative formation energies using the following Eq. (1);

$$E_{formation} = E(K_x[Cr_{0.84}Sb_{0.14}]O_2) - \frac{(1-x)E(K_0[Cr_{0.84}Sb_{0.14}]O_2) + xE(K_1[Cr_{0.84}Sb_{0.14}]O_2)}{2} \quad (1)$$

Moreover, based on lowest formation energies of each composition, we predicted the theoretical redox potentials of P3−KCSO using the following Eq. (2);

In the equation, *V* represents the average redox potential between K_{x2} $[Cr_{0.86}Sb_{0.14}]O_2$ and K_{x1} $[Cr_{0.86}Sb_{0.14}]O_2$, and *E[K]* and *F* refer to the formation energy of K metal and the Faraday constant, respectively. As shown in Fig. 2a, the computational results indicate that more than 0.5 mol K^+ can be reversibly de/intercalated at the P3−KCSO structure. It was verified that the theoretical redox potentials of P3−KCSO structure well matched with the experimentally measured charge/discharge curves at ~15 mA/g (Fig. 2b). To get a better understanding of the structural changes by variations in K content, we conducted theoretical investigations of the crystal structure and changes in the *c* lattice (Fig. 2c). As the K content decreases from 0.75 to 0.25 mol, the *c* lattice parameter of the P3−KCSO structure increases from ~18.46 Å to ~19.12 Å due to the repulsive force between adjacent oxygen atoms in the P3−KCSO structure.

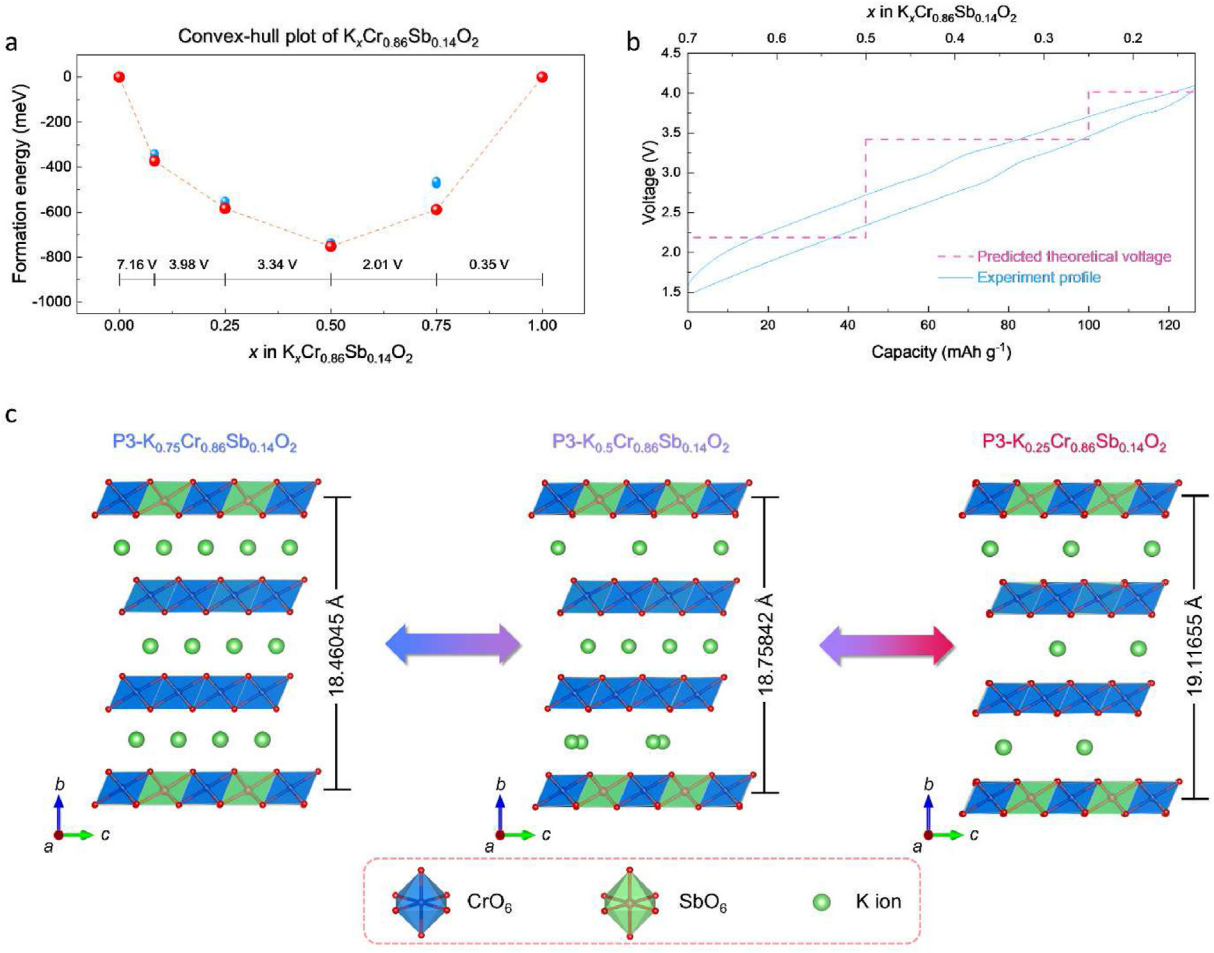

Fig. 2. (a) Convex-hull plot for the formation energy of P3-$K_xCr_{0.86}Sb_{0.14}O_2$ configurations ($0 \le x \le 1$) with theoretical voltage. (b) Comparison of the calculated redox potential of P3-$K_xCr_{0.86}Sb_{0.14}O_2$ and its experimentally measured cycle curves at 15 mA/g during initial charge/discharge process. (c) Predicted structural changes of P3-$K_xCr_{0.86}Sb_{0.14}O_2$ as a function of the K content ($0.25 \le x \le 0.75$) using first-principles calculations.

$$V = -\frac{E(K_{x_2}[Cr_{0.84}Sb_{0.14}]O_2) - E(K_{x_1}[Cr_{0.84}Sb_{0.14}]O_2) - (x_1 - x_2)E[K]}{(x_1 - x_2)F} \quad (2)$$

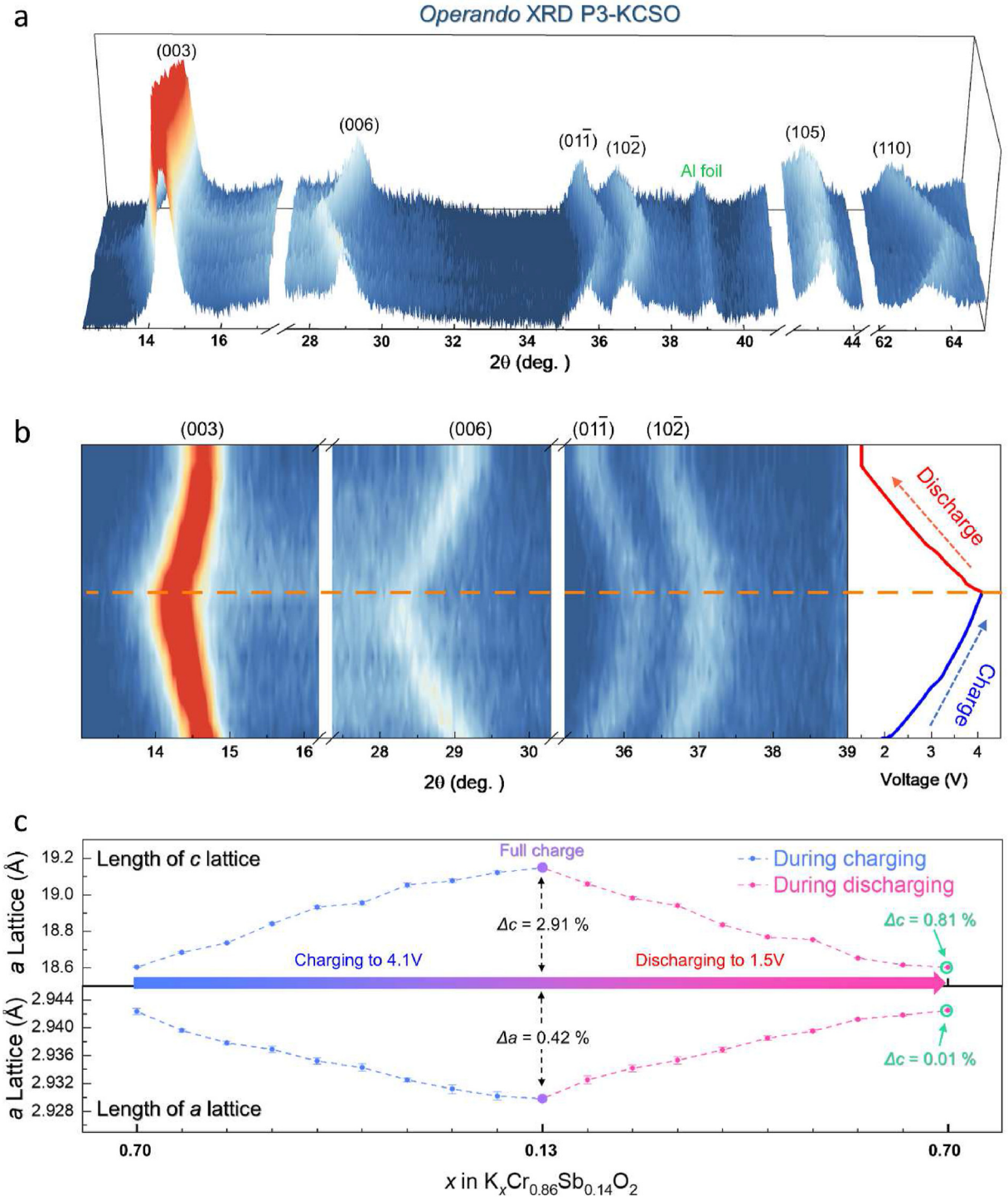

Fig. 3. (a) *Operando* XRD patterns of P3-$K_xCr_{0.86}Sb_{0.14}O_2$ (voltage range: 1.5–4.1 V). (b) Magnified views of P3-$K_xCr_{0.86}Sb_{0.14}O_2$. (c) Change in the *c* and *a* lattice parameter as a function of K content in P3-$K_xCr_{0.86}Sb_{0.14}O_2$.

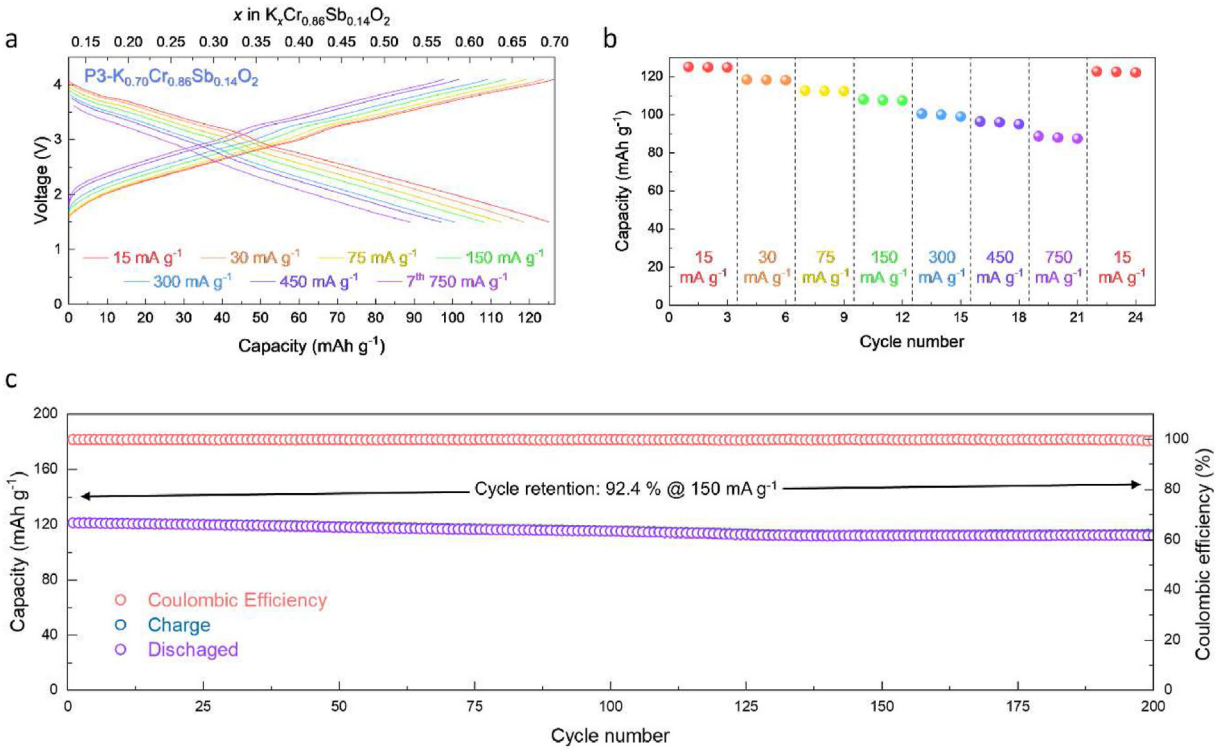

Fig. 4. (a) Charge/discharge profiles of P3-$K_xCr_{0.86}Sb_{0.14}O_2$ at various current densities in the voltage range of 1.5–4.1 V. (b) Power capability of P3-$K_xCr_{0.86}Sb_{0.14}O_2$ at various current densities. (c) Charge/discharge capacity and coulombic efficiency of P3-$K_xCr_{0.86}Sb_{0.14}O_2$ over 200 cycles at 150 mA/g.

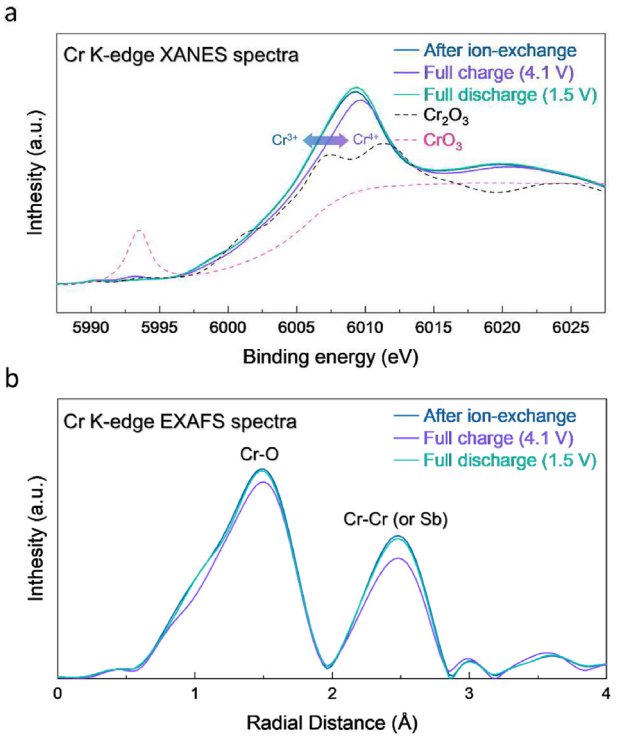

Fig. 5. (a) *Ex situ* Cr K-edge (a) XANES spectra and (b) EXAFS spectra of P3-$K_xCr_{0.86}Sb_{0.14}O_2$.

To confirm the first-principles calculation results on the structural changes during K^+ de/intercalation, we carried out *operando* XRD experiments. As shown in Fig. 3a–b, the peak positions of (003), (006), $(01\bar{1})$, $(10\bar{2})$, (105), and (110) planes were observed to shift during charging up to 4.1 V (vs. K^+/K) without the appearance of any new peaks, and returned to their original positions during discharging to 1.5 V. Moreover, intensities of the XRD pattern were recovered without severe structural degradation during cycling. These results indicate that the P3-type layered structure of P3–KCSO was stably maintained without any phase transition and exhibited high reversibility even after charging up to 4.1 V. In addition, we performed Rietveld refinement analyses on the *operando* XRD patterns of P3–KCSO to verify the high structural reversibility (Fig. 3c). It was verified that the *a* and *c* lattice parameters of P3–KCSO were changed from 2.9423 Å and 18.6060 Å to 2.9298 Å and 19.1478 Å ($\Delta a = 0.42\%$ $\Delta c = 2.91\%$) during charge. After discharge, they were well recovered to the original values. In terms of the volume, its change during charge was 2.04% (Fig. S3). Moreover, the a, c lattice parameters and volume were well recovered to the original value after cycling, which indicates the high structural stability of P3–$K_{0.70}[Cr_{0.86}Sb_{0.14}]O_2$.

Fig. 4a–b shows the electrochemical tests at various current densities of 15, 30, 75, 150, 300, 450, and 750 mA/g in the voltage range of 1.5–4.1 V. At 15 mA/g, the specific discharge capacity of P3–KCSO was 126.1 mAh/g with high Coulombic efficiency of above 98.7%, which indicates that irreversible reactions, such as formation of the solid electrolyte interface (SEI) layer, are negligibly occurred during initial discharge process of P3–KCSO. In addition, we measured the electrochemical properties based on the 1.0 M KPF_6 electrolyte and compared them with the properties based on the 0.5 M KPF_6 electrolyte. As shown in Fig. S4, it was confirmed that the charge capacities were larger than each discharge capacities under the KIB system using 1 M KPF_6 electrolyte, indicating that 1.0 M KPF_6 electrolyte can deliver worse electrochemical performances than 0.5 M KPF_6 electrolyte. This result is consistent with previous research that compared the electrochemical performance of

electrolytes with various molar ratios of KPF_6 [33–35]. Under the KIB system using 0.5 M KPF_6 electrolyte, P3–KCO delivered a discharge capacity of 115.5 mAh/g but had a much lower coulombic efficiency of 78.2% (Fig. S5). Importantly, the charge/discharge curve and the *dQ/dV* profile of P3–KCSO were smoother and much simpler compared to P3–KCO (Figs. S6–S7), indicating that the electrochemical behavior of P3–KCSO was less complex and structurally more stable than P3–KCO. In addition, the cathodic and anodic peaks are clearly verified in the *dQ/dV* profile of P3–KCSO, which indicates that not supercapacitor-like surface reaction but intercalation-based reaction in the structure occurred at P3–KCSO during charge/discharge. Even at a current density of 750 mA/g, furthermore, P3–KCSO exhibited a discharge capacity of ~88.9 mAh/g, corresponding to 71.1% of the capacity observed at 15 mA/g. In contrast, the discharge capacity of P3–KCO at 750 mA/g was only retained to 39.5% of the capacity delivered at 15 mA/g. Moreover, P3–KCSO demonstrated high cycle performance, as shown in Fig. 4c. At 150 mA/g, the capacity retention was ~92.4% after 200 cycles, and the coulombic efficiency was over 99% for all cycles. However, the P3–KCO only delivered a capacity retention of 37.9% compared with the initial capacity under the same condition (Fig. S8). These results suggest that the Sb substitution in the P3–KCSO structure can lead to outstanding power-capability and cycle-performance by enhancing structural stabilization. In addition, we compared the electrochemical performances of P3–KCSO with those of other various cathode materials of KIBs [16,26,36–41]. As shown in Table S5, it was clearly revealed P3–KCSO exhibited more outstanding electrochemical performances than other cathode materials for KIBs, which indicates that P3–KCSO exhibits high competitiveness as the promising cathode for KIBs.

Additionally, we investigated the reaction mechanism of P3–KCSO during K^+ de/intercalation using *ex situ* synchrotron-based X-ray absorption spectroscopy (XAS) analyses. As shown in Fig. 5a, the Cr K-edge XANES spectra of P3–KCSO shifted to a higher energy level during charging, followed by a return to a state that very similar to the original state upon discharging. These results indicate that the occurrence of a reversible Cr^{3+}/Cr^{4+} redox reaction in P3–KCSO during K^+ de/intercalation. Moreover, through *ex-situ* X-ray absorption fine structure (EXAFS) analyses (Fig. 5b), it was revealed the bond length of Cr–O decreased after charge and it was recovered to its original length after discharge. This result strongly implies the high structural reversibility of P3–KCSO.

4. Conclusion

In this work, we demonstrated that the substitution of Sb (0.14 mol) into the crystal structure can enhance the electrochemical performances of P3-K_xCrO_2 (P3–KCO). P3–$K_{0.70}$ $[Cr_{0.86}Sb_{0.14}]O_2$ (P3–KCSO) delivered a specific capacity of 126.1 mAh/g at 15 mA/g, corresponding to the de/intercalation of 0.51 mol of K^+ ions from/into the structure. The charge-discharge voltage profiles of P3–KCSO are smoother than those of P3–KCO, indicating that Sb substitution can suppress the irreversible phase transition during the (de) potassiation process. Moreover, P3–KCSO showed high power capability with a specific capacity of 88.9 mAh/g at 750 mA/g, corresponding to 71.1% of the capacity measured at 15 mA/g. Furthermore, after 200 cycles, the capacity retention of discharge was maintained to 92.4% with high coulombic efficiency of >99% at 150 mA/g. These excellent electrochemical performances of P3–KCSO were mainly attributed to the improved structural stability with a highly reversible Cr^{3+}/Cr^{4+} redox reaction. The reversible K^+ storage mechanism of P3–KCSO was confirmed by a combined study of first-principles calculations and various experiments, including cluster expansion method-based calculations, *operando* XRD, and *ex situ* XAS analysis. We believe that these findings will provide new inspiration for the development of high-performance cathode materials for potassium-ion batteries.

CRediT author statement

Wonseok Ko: Conceptualization, Software, Validation, Visualization, Investigation, Resources, Writing–Original, Writing–Review & Editing Formal analysis and Methodology and Visualization. **Junseong Kim**: Validation, Visualization, Investigation and Resources. **Jungmin Kang**: Investigation. **Hyunyoung Park**: Investigation, Software and Methodology. **Yongseok Lee**: Investigation. **Jinho Ahn**: Validation. **Bonyoung Ku**: Validation. **Myungeun Choi**: Validation. **Hobin Ahn**: Validation. **Gwangeon Oh**: Investigation. **Jang-Yeon Hwang**: Conceptualization, Writing-Review & Editing, Funding acquisition. **Jongsoon Kim**: Project administration, Conceptualization, Supervision, Data curation, Writing-Review & Editing, Funding acquisition.

Declaration of competing interest

The authors declare that they have no known competing financial interests or personal relationships that could have appeared to influence the work reported in this paper.

Data availability

Data will be made available on request.

Acknowledgement

This work was supported by the National Research Foundation of Korea (NRF) grant funded by the Korea government (MSIT, Ministry of Science and ICT) (NRF-2021R1A2C1014280, NRF–2022R1C1C1011058) and Korea Institute of Science and Technology (KIST) Institutional Program (No. 2E32581-23-092).

Appendix A. Supplementary data

Supplementary data to this article can be found online at https://doi.org/10.1016/j.mtener.2023.101356.

References

[1] K. Caldeira, J.F. Kasting, Insensitivity of global warming potentials to carbon dioxide emission scenarios, Nature 366 (1993) 251–253, https://doi.org/10.1038/366251a0.
[2] M. Armand, J.-M. Tarascon, Building better batteries, Nature 451 (2008) 652–657, https://doi.org/10.1038/451652a.
[3] D. Larcher, J.M. Tarascon, Towards greener and more sustainable batteries for electrical energy storage, Nat. Chem. 7 (2015) 19–29, https://doi.org/10.1038/nchem.2085.
[4] W. Ko, H. Park, J.H. Jo, Y. Lee, J. Kang, Y.H. Jung, T.-Y. Jeon, S.-T. Myung, J. Kim, Unveiling yavapaiite-type $KFe(SO_4)_2$ as a new Fe-based cathode with outstanding electrochemical performance for potassium-ion batteries, Nano Energy 66 (2019) 104184, https://doi.org/10.1016/j.nanoen.2019.104184.
[5] W. Ko, J.-K. Yoo, H. Park, Y. Lee, I. Kang, J. Kang, J.H. Jo, J.U. Choi, J. Hong, S.-T. Myung, J. Kim, Exceptionally high-energy tunnel-type $V_{1.5}Cr_{0.5}O_{4.5}H$ nanocomposite as a novel cathode for Na-ion batteries, Nano Energy 77 (2020) 105175, https://doi.org/10.1016/j.nanoen.2020.105175.
[6] S.W. Kim, D.H. Seo, X. Ma, G. Ceder, K. Kang, Electrode materials for rechargeable sodium-ion batteries: potential alternatives to current lithium-ion batteries, Adv. Energy Mater. 2 (2012) 710–721, https://doi.org/10.1002/aenm.201200026.
[7] W. Hong, Y. Zhang, L. Yang, Y. Tian, P. Ge, J. Hu, W. Wei, G. Zou, H. Hou, X. Ji, Carbon quantum dot micelles tailored hollow carbon anode for fast potassium and sodium storage, Nano Energy 65 (2019) 104038, https://doi.org/10.1016/j.nanoen.2019.104038.
[8] Y. Liu, Z. Tai, Q. Zhang, H. Wang, W.K. Pang, H.K. Liu, K. Konstantinov, Z. Guo, A new energy storage system: rechargeable potassium-selenium battery, Nano Energy 35 (2017) 36–43, https://doi.org/10.1016/j.nanoen.2017.03.029.

[9] Q. Yang, Z. Wang, W. Xi, G. He, Tailoring nanoporous structures of Ge anodes for stable potassium-ion batteries, Electrochem. Commun. 101 (2019) 68–72, https://doi.org/10.1016/j.elecom.2019.02.016.
[10] J.C. Pramudita, D. Sehrawat, D. Goonetilleke, N. Sharma, An initial review of the status of electrode materials for potassium-ion batteries, Adv. Energy Mater. 7 (2017) 1–21, https://doi.org/10.1002/aenm.201602911.
[11] Y. Marcus, Thermodynamic functions of transfer of single ions from water to nonaqueous and mixed solvents: Part 3 - standard potentials of selected electrodes, Pure Appl. Chem. 57 (2007) 1129–1132, https://doi.org/10.1351/pac198557081129.
[12] F. Wang, L.E. Blanc, Q. Li, A. Faraone, X. Ji, H.H. Chen-Mayer, R.L. Paul, J.A. Dura, E. Hu, K. Xu, L.F. Nazar, C. Wang, Quantifying and suppressing proton intercalation to enable high-voltage Zn-ion batteries, Adv. Energy Mater. (2021) 1–11, https://doi.org/10.1002/aenm.202102016, 2102016.
[13] H. Duc Pham, C. Padwal, J.F.S. Fernando, T. Wang, T. Kim, D. Golberg, D.P. Dubal, Back-integration of recovered graphite from waste-batteries as ultra-high capacity and stable anode for potassium-ion battery, Batter. Supercaps. 5 (2022), https://doi.org/10.1002/batt.202100335.
[14] A. Metrot, D. Guerard, D. Billaud, A. Herold, New results about the sodium-graphite system, Synth. Met. 1 (1980) 363–369, https://doi.org/10.1016/0379-6779(80)90071-5.
[15] N. Adhoum, J. Bouteillon, D. Dumas, J.C. Poignet, Electrochemical insertion of sodium into graphite in molten sodium fluoride at 1025 °C, Electrochim. Acta 51 (2006) 5402–5406, https://doi.org/10.1016/j.electacta.2006.02.019.
[16] J.U. Choi, J. Kim, J.-Y. Hwang, J.H. Jo, Y.-K. Sun, S.-T. Myung, $K_{0.54}[Co_{0.5}Mn_{0.5}]O_2$: new cathode with high power capability for potassium-ion batteries, Nano Energy 61 (2019) 284–294, https://doi.org/10.1016/j.nanoen.2019.04.062.
[17] M. Gu, A.M. Rao, J. Zhou, B. Lu, In situ formed uniform and elastic SEI for high-performance batteries, Energy Environ. Sci. 16 (2023) 1166–1175, https://doi.org/10.1039/D2EE04148K.
[18] X. Yi, Y. Feng, A.M. Rao, J. Zhou, C. Wang, B. Lu, Quasi-solid aqueous electrolytes for low-cost sustainable alkali-metal batteries, Adv. Mater. (2023), https://doi.org/10.1002/adma.202302280.
[19] H. Park, Y. Lee, W. Ko, M. Choi, B. Ku, H. Ahn, J. Kim, J. Kang, J.-K. Yoo, J. Kim, Review on cathode materials for sodium- and potassium-ion batteries: structural design with electrochemical properties, Batter. Supercaps. 6 (2023) e202200486, https://doi.org/10.1002/batt.202200486.
[20] L. Wu, H. Fu, S. Li, J. Zhu, J. Zhou, A.M. Rao, L. Cha, K. Guo, S. Wen, B. Lu, Phase-engineered cathode for super-stable potassium storage, Nat. Commun. 14 (2023) 644, https://doi.org/10.1038/s41467-023-36385-4.
[21] J. Bao, W. Deng, J. Liu, C.-F. Sun, Ultrafast-kinetics, ultralong-cycle-life, bifunctional inorganic open-framework for potassium-ion batteries, Energy Storage Mater. 42 (2021) 806–814, https://doi.org/10.1016/j.ensm.2021.08.029.
[22] Z. Wang, W. Zhuo, J. Li, L. Ma, S. Tan, G. Zhang, H. Yin, W. Qin, H. Wang, L. Pan, A. Qin, W. Mai, Regulation of ferric iron vacancy for Prussian blue analogue cathode to realize high-performance potassium ion storage, Nano Energy 98 (2022) 107243, https://doi.org/10.1016/j.nanoen.2022.107243.
[23] Y. Li, C. Yang, F. Zheng, Q. Pan, Y. Liu, G. Wang, T. Liu, J. Hu, M. Liu, Design of TiO_2eC hierarchical tubular heterostructures for high performance potassium ion batteries, Nano Energy 59 (2019) 582–590, https://doi.org/10.1016/j.nanoen.2019.03.002.
[24] X. Zhang, Y. Yang, X. Qu, Z. Wei, G. Sun, K. Zheng, H. Yu, F. Du, Layered P2-type $K_{0.44}Ni_{0.22}Mn_{0.78}O_2$ as a high-performance cathode for potassium-ion batteries, Adv. Funct. Mater. 29 (2019) 1905679, https://doi.org/10.1002/adfm.201905679.
[25] S. Komaba, T. Hasegawa, M. Dahbi, K. Kubota, Potassium intercalation into graphite to realize high-voltage/high-power potassium-ion batteries and potassium-ion capacitors, Electrochem. Commun. 60 (2015) 172–175, https://doi.org/10.1016/j.elecom.2015.09.002.
[26] J.-Y. Hwang, J. Kim, T.-Y. Yu, S.-T. Myung, Y.-K. Sun, Development of P3-$K_{0.69}CrO_2$ as an ultra-high-performance cathode material for K-ion batteries, Energy Environ. Sci. 11 (2018) 2821–2827, https://doi.org/10.1039/C8EE01365A.
[27] Q.Q. Qiu, Z. Shadike, Q.C. Wang, X.Y. Yue, X.L. Li, S.S. Yuan, F. Fang, X.J. Wu, A. Hunt, I. Waluyo, S.M. Bak, X.Q. Yang, Y.N. Zhou, Improving the electrochemical performance and structural stability of the $LiNi_{0.8}Co_{0.15}Al_{0.05}O_2$ cathode material at high-voltage charging through Ti substitution, ACS Appl. Mater. Interfaces 11 (2019) 23213–23221, https://doi.org/10.1021/acsami.9b05100.
[28] W. Ko, M.-K. Cho, J. Kang, H. Park, J. Ahn, Y. Lee, S. Lee, S. Lee, K. Heo, J. Hong, J.-K. Yoo, J. Kim, Exceptionally increased reversible capacity of O3-type $NaCrO_2$ cathode by preventing irreversible phase transition, Energy Storage Mater. 46 (2022) 289–299, https://doi.org/10.1016/j.ensm.2022.01.023.
[29] Y. Chen, Y. Xu, X. Sun, C. Wang, Effect of Al substitution on the enhanced electrochemical performance and strong structure stability of $Na_3V_2(PO_4)_3$/C composite cathode for sodium-ion batteries, J. Power Sources 375 (2018) 82–92, https://doi.org/10.1016/j.jpowsour.2017.11.043.
[30] P. Cui, Z. Jia, L. Li, T. He, Preparation and characteristics of Sb-doped $LiNiO_2$ cathode materials for Li-ion batteries, J. Phys. Chem. Solid. 72 (2011) 899–903, https://doi.org/10.1016/j.jpcs.2011.04.013.
[31] Z. Chen, Q. Liu, X. Yan, H. Zhu, J. Liu, J. Duan, Y. Wang, Suppression and mechanism of voltage decay in Sb-doped lithium-rich layered oxide cathode materials, J. Phys. Chem. Lett. 13 (2022) 8214–8220, https://doi.org/10.1021/acs.jpclett.2c02070.
[32] V.I. Anisimov, F. Aryasetiawan, A.I. Lichtenstein, First-principles calculations of the electronic structure and spectra of strongly correlated systems: the LDA + U method, J. Phys. Condens. Matter 9 (1997) 767–808, https://doi.org/10.1088/0953-8984/9/4/002.
[33] Y. Lei, D. Han, J. Dong, L. Qin, X. Li, D. Zhai, B. Li, Y. Wu, F. Kang, Unveiling the influence of electrode/electrolyte interface on the capacity fading for typical graphite-based potassium-ion batteries, Energy Storage Mater. 24 (2020) 319–328, https://doi.org/10.1016/j.ensm.2019.07.043.
[34] W. Luo, J. Wan, B. Ozdemir, W. Bao, Y. Chen, J. Dai, H. Lin, Y. Xu, F. Gu, V. Barone, L. Hu, Potassium ion batteries with graphitic materials, Nano Lett. 15 (2015) 7671–7677, https://doi.org/10.1021/acs.nanolett.5b03667.
[35] J. Kang, W. Ko, H. Park, Y. Lee, J.H. Jo, J.U. Choi, S.-T. Myung, J. Kim, High-power rhombohedral-$Fe_2(SO_4)_3$ with outstanding cycle-performance as Fe-based cathode for K-ion batteries, Energy Storage Mater. 33 (2020) 276–282, https://doi.org/10.1016/j.ensm.2020.08.024.
[36] Z. Xiao, F. Xia, L. Xu, X. Wang, J. Meng, H. Wang, X. Zhang, L. Geng, J. Wu, L. Mai, Suppressing the jahn–teller effect in Mn-based layered oxide cathode toward long-life potassium-ion batteries, Adv. Funct. Mater. 32 (2022) 2108244, https://doi.org/10.1002/adfm.202108244.
[37] Z. Xiao, J. Meng, F. Xia, J. Wu, F. Liu, X. Zhang, L. Xu, X. Lin, L. Mai, K^+ modulated K^+/vacancy disordered layered oxide for high-rate and high-capacity potassium-ion batteries, Energy Environ. Sci. 13 (2020) 3129–3137, https://doi.org/10.1039/D0EE01607A.
[38] L. Duan, Y. Xu, Z. Zhang, J. Xu, J. Liao, J. Xu, Y. Sun, Y. He, X. Zhou, A high-performance cathode for potassium-ion batteries based on uniform P3-type $K_{0.5}Mn_{0.8}Co_{0.1}Ni_{0.1}O_2$ porous microcuboids, J. Mater. Chem. A. 9 (2021) 22820–22826, https://doi.org/10.1039/D1TA07108D.
[39] J.U. Choi, J. Kim, J.H. Jo, H.J. Kim, Y.H. Jung, D.-C. Ahn, Y.-K. Sun, S.-T. Myung, Facile migration of potassium ions in a ternary P3-type $K_{0.5}[Mn_{0.8}Fe_{0.1}Ni_{0.1}]O_2$ cathode in rechargeable potassium batteries, Energy Storage Mater. 25 (2020) 714–723, https://doi.org/10.1016/j.ensm.2019.09.015.
[40] B. Peng, Y. Li, J. Gao, F. Zhang, J. Li, G. Zhang, High energy K-ion batteries based on P3-Type $K_{0.5}MnO_2$ hollow submicrosphere cathode, J. Power Sources 437 (2019) 226913, https://doi.org/10.1016/j.jpowsour.2019.226913.
[41] N. Naveen, S.C. Han, S.P. Singh, D. Ahn, K.-S. Sohn, M. Pyo, Highly stable P′3-$K_{0.8}CrO_2$ cathode with limited dimensional changes for potassium ion batteries, J. Power Sources 430 (2019) 137–144, https://doi.org/10.1016/j.jpowsour.2019.05.017.